RSC Advances

ROYAL SOCIETY OF CHEMISTRY

www.rsc.org/advances

RSCPublishing

COMMUNICATION

Fabrication and characteristics of a high-capacity $LiNi_{0.8}Co_{0.15}Al_{0.05}O_2$ with the monodisperse yolk-shell spherical precursors by a facile method

Cite this: DOI: 10.1039/x0xx00000x

Received ooth January 2012,
Accepted ooth January 2012

DOI: 10.1039/x0xx00000x

www.rsc.org/

Huazhen Yang,[a] Panxing Liu, [a] Qinglin Chen, [a] Xuewen Liu, [a] Yanwen Lu, [a] Shuangfei Xie, [a] Liang Ni, [a] Xingyun Wu, [a] Muyang Peng, [a] Yanbin Chen, [b] Yuefeng Tang, [a]* Yanfeng Chen [a]

The structure of yolk–shell microspheres is attractive since it exhibits excellent structural stability during lithiation, and the monodisperse crumpled yolk–shell spherical precursors of $LiNi_{0.8}Co_{0.15}Al_{0.05}O_2$ were obtained via a general and simple supersonic atomization method. After mixed with $LiNO_3$, this cathode material showed a high discharge capacity about 225.9mAh g^{-1} and showed a good cycle performance at 0.2C, which is higher than previously reported.

$LiNiO_2$ was considered to replace $LiCoO_2$ as the cathode applied in commercial Li-ion batteries, for its lower cost and higher reversible capacity. [1-3] However, comparing to $LiCoO_2$, poor thermodynamic stability [4] limited its application. Therefore, Ni-rich $LiNi_{1-x}Co_xO_2$ ($0<x<1$) [5] was developed to solve the security problem of $LiNiO_2$, [6] and Al-doping was reported to improve its cycling stability. [7-11] $LiNi_{0.8}Co_{0.15}Al_{0.05}O_2$ is one of most applicable cathode materials for advanced lithium ion batteries. [12]

However, to meet the requirement of $LiNi_{0.8}Co_{0.15}Al_{0.05}O_2$ applications in the future, a lot of work to precisely control its shape and size is needed, and monodisperse structure can improve the consistency of performance of lithium ion battery. Many progresses have been made to prepare $LiNi_{0.8}Co_{0.15}Al_{0.05}O_2$ precursor powers, including co-precipitation, [13-18] PVA precursor method [19] and spay pyrolysis. [20] The structure of yolk–shell microspheres is attractive since it exhibits excellent structural stability during lithiation, [21-23] which shows a higher capacity than a solid or hollow structure, but there are no reports about synthesis of the monodisperse precursors of $LiNi_{0.8}Co_{0.15}Al_{0.05}O_2$ with yolk-shell structure before.

Herein, the monodisperse precursors of $LiNi_{0.8}Co_{0.15}Al_{0.05}O_2$ with uniform shape and size were successfully obtained via supersonic atomization method. Interestingly, the precursor powders are yolk-shell spherical structure and verified by Transmission Electron Microscopy (TEM), and these monodisperse yolk-shell structures showed a high capacity after mixed with $LiNO_3$.

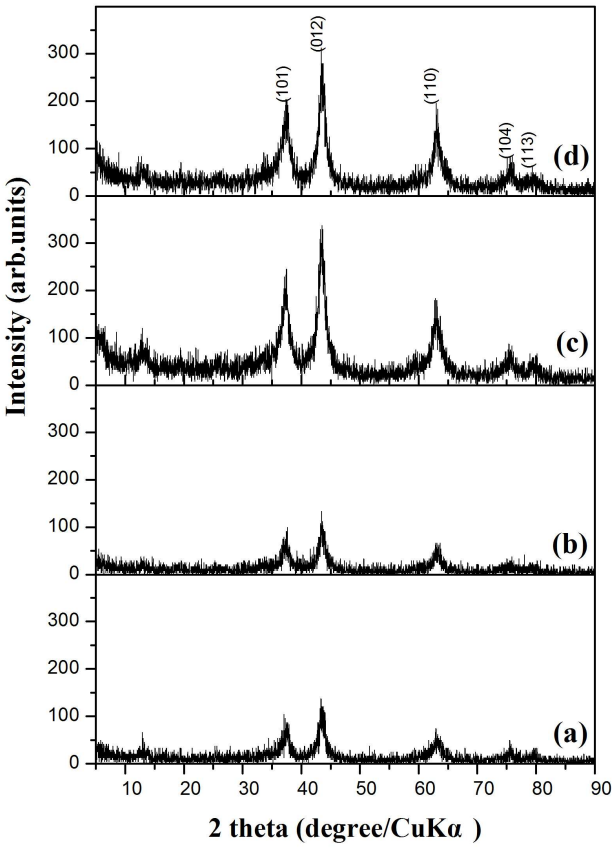

Fig. 1 XRD patterns of oxide precursors prepared at different dried temperature (a) 400 °C, (b) 450 °C, (c) 500 °C, (d) 550 °C.

The oxide precursor powders of $LiNi_{0.8}Co_{0.15}Al_{0.05}O_2$ were prepared through a ultrasonic atomizing method using aqueous solutions of $Ni(NO_3)_2$•$6H_2O$(98%), $Co(NO_3)_2$•$6H_2O$(98%) and

$Al(NO_3)_2$•$9H_2O$ (98%) in the molar ratio of Ni/Co/Al=0.8/0.15/0.05. The 1.5 mol/L mixed solution was atomized to form droplets dried at 400 °C, 450 °C, 500 °C and 550 °C in air, respectively. The mixture of the oxide precursor powders and $LiNO_3$ was sintered at 850 °C at a rate of 100 mL min^{-1} under an air flow. The crystalline phase and structure of the prepared samples were identified by X-ray diffraction (XRD, Rigaku D-Max-RA) equipped with a diffracted-beam monochromator (Cu Kα radiation) at room temperature. The surface morphology and microstructure were also characterized using scanning electron microscopy (SEM, QUANTA-200) and transmission electron microscopy (TEM, JEOL-2100). The Brunauer, Emmett, and Teller (BET) surface area was analyzed by using nitrogen-hydrogen mixture from (Quantachrome MONOSORB). The composition of the prepared sample was confirmed by using inductively coupled plasma (ICP, PekinElmer-Optima-5300DV). The initial charge and discharge curves of the cathode powders prepared from the oxide precursors at a rate of 0.1 C between 2.8 and 4.5 V (1 C rate was set as 180 mAh g^{-1}) at the room temperature and 60 °C was run and controlled by a Neware BTS-5V5MA-S1 and MACCOR S4000 Startup Battery Test System instrument.

Fig. 1 clearly showed the crystal structure of the samples prepared at 400 °C, 450 °C, 500 °C and 550 °C, and all the diffraction peaks can be in good agreement with the patterns of NiO (JCPDS No.: 44-1159). And the intensities of these peaks increased with the increasing temperature, which pointed that crystallinity of the powders increased as the dried temperature increased.

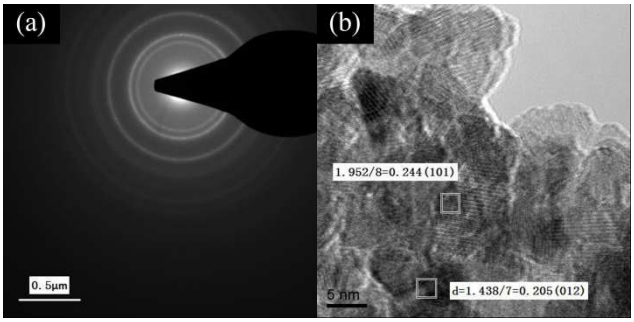

Fig. 4 TEM micrographs of the oxide precursors prepared at 550 oC (a) SAED pattern, (b) HRTEM micrograph.

TEM was employed to further verify the crystal structure of the precursor samples. Corresponding selected-area electron diffraction (SAED) pattern of precursors prepared at 550 °C confirmed its polycrystalline structure (Fig. 2(a)). As marked in Fig. 2(b), the high resolution TEM (HRTEM) micrograph of the sample, with interplanar spacing of approximately 0.244 nm between neighboring [1 0 1] planes and 0.205 nm between neighboring [0 1 2] planes, these indexed patterns were in good agreement with the XRD described in Fig. 1(d).

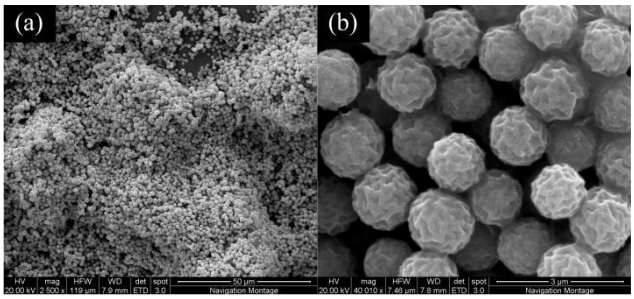

Fig. 3 SEM micrographs of the oxide precursors prepared at 400 °C (a) Overall morphology, (b) low-magnification.

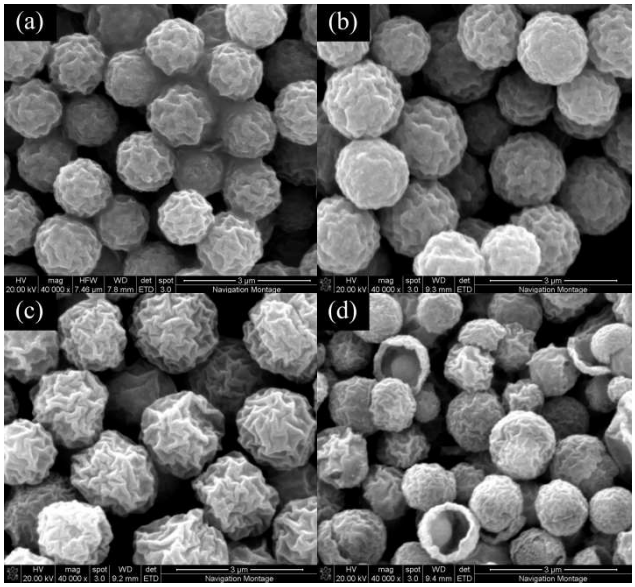

Fig. 4 SEM micrographs of oxide precursors prepared at different dried temperature (a) 400 °C, (b) 450 °C, (c) 500 °C, (d) 550 °C.

We could repeat the process of the whole experiment to successfully produce monodisperse precursor powder at different dried temperatures, which are shown in Fig. 4, and highly uniform and monodisperse spheres were obtained. Obviously, the average diameter and crumpled degree of the microspheres were indeed increased gradually as the dried temperature increased from 400 °C to 500 °C. Interestingly, Fig. 4(d) clearly showed some cracks and broken shells in microspheres while the dried temperature reached 550 °C, and some of the smaller spheres inside the broken particles suggested the possible yolk-shell structures.

Table 1 BET data of the oxide precursors prepared at different dried temperature (A) 400 °C, (B) 450 °C, (C) 500 °C, (D) 550 °C.

Sample	Mass (g)	Surface area (m^2)	Specific surface area (m^2 g^{-1})
(A)	0.1354	0.51	3.77
(B)	0.4344	1.78	4.09
(C)	0.2074	0.95	4.58
(D)	0.1490	0.76	5.10

Table 1 showed the changes in the specific surface area of precursors prepared at different dried temperatures. Brunauer, Emmett, and Teller (BET) measurements indicated specific surface areas of the samples increased from 3.77 m^2 g^{-1} to 5.10 m^2 g^{-1} as the dried temperature increased, because the crumpled degree of the microspheres indeed increased gradually from 400 °C to 550 °C as shown in Fig. 4.

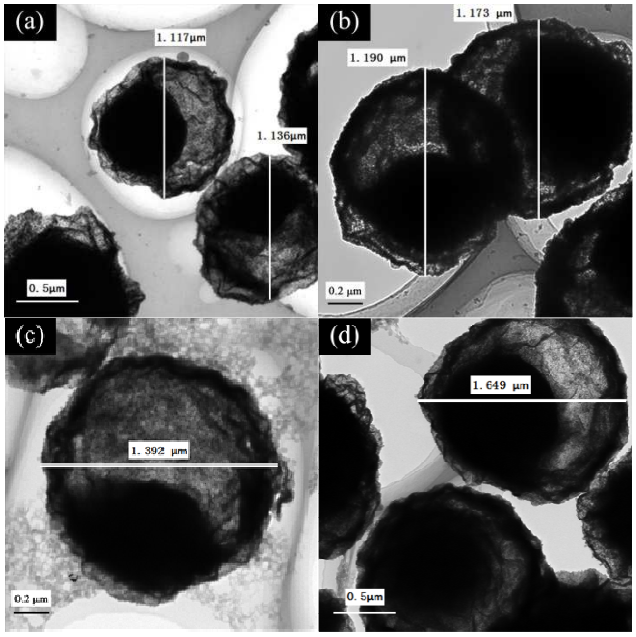

Fig. 5 TEM micrographs of oxide precursors prepared at different dried temperature (a) 400 ^{o}C overall morphology, (b) 450 ^{o}C, (c) 500 ^{o}C, (d) 550 ^{o}C.

TEM samples were prepared to prove that the interior of the microspheres are similar to those yolk-shell structures shown in the SEM micrograph at Fig. 5(d) 550 ^{o}C, and the stark contrast of colour confirmed that the gap between the shell and the inner core. From Fig. 5 observations, it is found that the diameters of the yolk-shell microspheres indeed increased gradually from ~1.1 μm to ~1.6 μm as the dried temperature increased, in good accordance with the observation in Fig. 4.

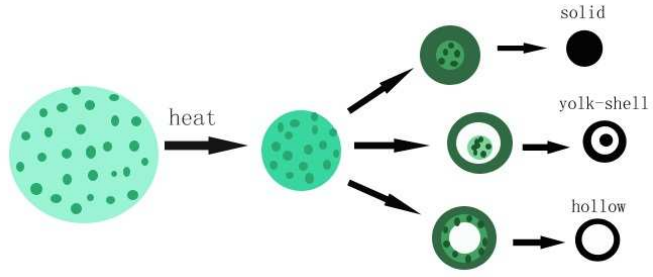

Fig. 6 The formation mechanism of the yolk-shell powders

As shown in Figure. 6, a spherical shell formed after water in the surface evaporated in heat. After the formation of the spherical shell, if the water evaporation rate near the surface of the droplet was greater than or equal to the water evaporation rate near the center, the remaining solution inside the droplet would dry close to the dried sphere shell and form solid spherical particles. Otherwise, the formation mechanism could be divided into the following two cases. In the first case, the remaining solution inside the droplet dried closely to the outside shell and formed the hollow structure. In the second case, the remaining solution dried solely and formed a smaller sphere inside the spherical shell. We can adjust the initial concentration of the mixed solution to control the diffusion rate of outward and inward layers in oxide spheres, so we can obtain the yolk-shell structure powders.

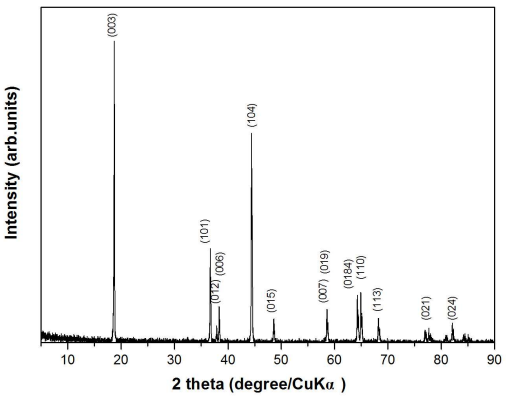

Fig. 7 An XRD pattern of the $LiNi_{0.8}Co_{0.15}Al_{0.05}O_2$ sintered at 850 ^{o}C at a rate of 100 mL min^{-1} under an air flow.

The mixture of $LiNi_{0.8}Co_{0.15}Al_{0.05}O_2$ precursors prepared at 400 ^{o}C ~ 550 ^{o}C and $LiNO_3$ was sintered at 850 ^{o}C at a rate of 100 mL min^{-1} under an air flow to obtain the $LiNi_{0.8}Co_{0.15}Al_{0.05}O_2$ powders, and the crystalline phase and structure of the $LiNi_{0.8}Co_{0.15}Al_{0.05}O_2$ were shown in Fig.7, all the diffraction peaks can be in good agreement with the patterns of $LiNiO_2$ (JCPDS No.: 74-0919). So this research provided a facile method to obtain a high-capacity lithium ion battery cathode material.

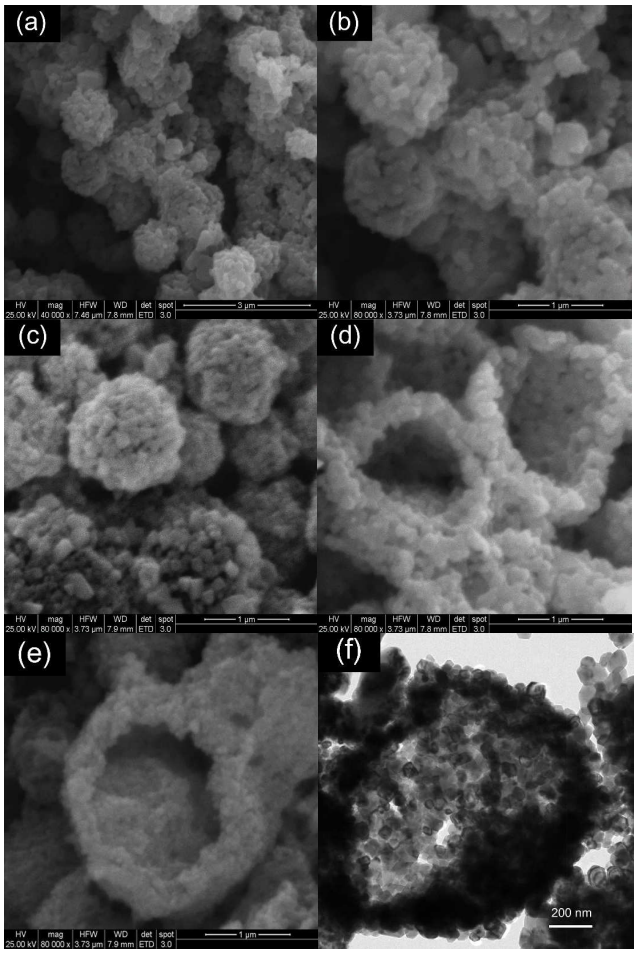

Fig. 8 SEM micrographs of the $LiNi_{0.8}Co_{0.15}Al_{0.05}O_2$ prepared by precursor powders dried at different temperature (a) 400 °C at overall morphology, (b) 400 °C at low-magnification,(c) 450 °C, (d) 500 °C, (e) 550 °C, TEM micrographs of (f) 550 °C

Table 2 BET data of the $LiNi_{0.8}Co_{0.15}Al_{0.05}O_2$ prepared by precursor powders dried at different temperature (A) 400 °C, (B) 450 °C, (C) 500 °C, (D) 550 °C

Sample	Mass (g)	Surface area (m^2)	Specific surface area ($m^2\ g^{-1}$)
(A)	0.2177	2.42	11.12
(B)	0.2508	2.87	11.44
(C)	0.2431	3.06	12.59
(D)	0.3095	3.10	10.02

To obtain the $LiNi_{0.8}Co_{0.15}Al_{0.05}O_2$, we used the mixture of the precursor powders dried at 400 °C~550 °C and $LiNO_3$ sintered at 850 °C at the rate of 100 mL min^{-1} under an air flow. As shown in Fig. 8(a), the sintered particles remained the spherical structure as the precursor particles, and the diameters of the microspheres indeed increased as the dried temperature increased, in good accordance with the precursor particles shown from Fig. 8. Obviously, the smaller spheres inside the broken particles suggested the sintered particles maybe remained the yolk-shell structure as the precursor particles. In order to prove the possible conclusion, the TEM samples were prepared as shown in Fig. 8(f) and confirmed the $LiNi_{0.8}Co_{0.15}Al_{0.05}O_2$ had the yolk-shell structure in good accordance with the precursor powders. The BET measurements as shown in Table 2 indicated the $LiNi_{0.8}Co_{0.15}Al_{0.05}O_2$ samples had larger specific surface areas than precursor powders and the sample C had the largest specific surface area about 12.59 $m^2\ g^{-1}$.

Table 3 The chemical composition analysis of the $LiNi_{0.8}Co_{0.15}Al_{0.05}O_2$ prepared by precursor powders at different dried temperature (A) 400 °C, (B) 450 °C, (C) 500 °C, (D) 550 °C by ICP

Sample	Li (mg L^{-1})	Ni (mg L^{-1})	Co (mg L^{-1})	Al (mg L^{-1})
(A)	5.41	36.8	6.58	0.91
(B)	3.52	23.6	4.24	0.62
(C)	4.69	31.7	5.58	0.88
(D)	3.69	24.3	4.29	0.67

The ICP analysis was done to confirm the composition of $LiNi_{0.8}Co_{0.15}Al_{0.05}O_2$ yolk-shell structure after calcination at the high temperature of 850 °C for 15h, and the measured atom ratios of Li : Ni : Co : Al in these four samples were all about 1 : 0.8 : 0.15 : 0.05. The results were in good accordance with the $LiNi_{0.8}Co_{0.15}Al_{0.05}O_2$ composition, which implied that the oxide precursors and $LiNO_3$ were homogeneously reacted at 850 °C.

Fig. 9 exhibited the initial charge/discharge curves of the mixture of the oxide precursor powders and $LiNO_3$ sintered at temperature of 850 °C for 15 h at a rate of 100 mL min^{-1} under an air flow. As listed on Table 4, precursor powders prepared at 550 °C showed an initial discharge capacity about 202.4 mAh g^{-1} at 0.1C, this result may be due to the broken yolk-shell shells as shown in Figure 4d. And the initial discharge capacity of sample D (dried at 500 °C) reached 225.9 mAh g^{-1} which is higher than previously reported. And the result implied that the sample with higher BET surface area had higher irreversible capacity during the first cycle.

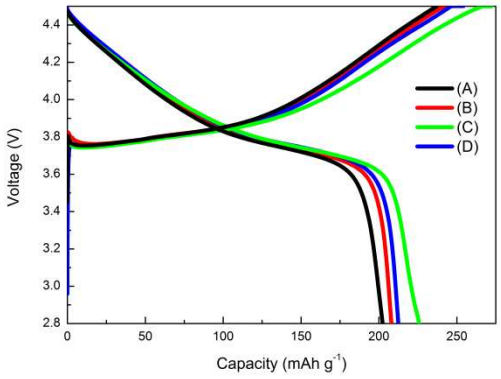

Fig. 9 Initial charge/discharge curves of the $LiNi_{0.8}Co_{0.15}Al_{0.05}O_2$ prepared by precursor powders at different dried temperature (A) 400 °C, (B) 450 °C, (C) 500 °C, (D) 550 °C tested at the room temperature (0.1C).

Table 4 Initial charge/ discharge capacity and efficiencies of the mixture of the $LiNi_{0.8}Co_{0.15}Al_{0.05}O_2$ prepared by precursor powders at different dried temperature (A) 400 °C, (B) 450 °C, (C) 500 °C, (D) 550 °C tested at the room temperature (0.1C).

Sample	Initial charge capacity(mAh g^{-1})	Initial discharge capacity(mAh g^{-1})	Efficiency (%)
(A)	246.9	208.0	84.26
(B)	254.3	212.5	83.54
(C)	272.4	225.9	82.93
(D)	242.4	202.4	83.51

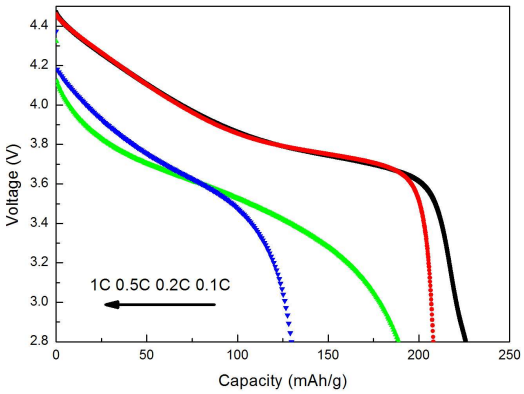

Fig. 10 Initial discharge curves of the mixture of the $LiNi_{0.8}Co_{0.15}Al_{0.05}O_2$ prepared by precursor powders at different dried at 500 °C at different discharge rates tested at the room temperature.

Fig. 10 showed the initial discharge capacities of the sample C at different discharge rates, which was prepared by precursor powders dried at 500 °C Precursor powders prepared at 550 °C. When the discharge current density varies from 0.1 C to 1 C, the initial discharge capacity of sample C, faded from 225.9 mAh g^{-1} to 129.7 mAh g^{-1}. But it showed a good cycle performance, the cycle performance curves of the $LiNi_{0.8}Co_{0.15}Al_{0.05}O_2$ at the rate of 0.2C

under the room temperature. As shown in the Fig. 11, the capacity of sample C only faded from 208.0 mAh g^{-1} to 185.9 mAh g^{-1} after 49 cycles and showed a good cycle performance of 89.38 % capacity retention rate.

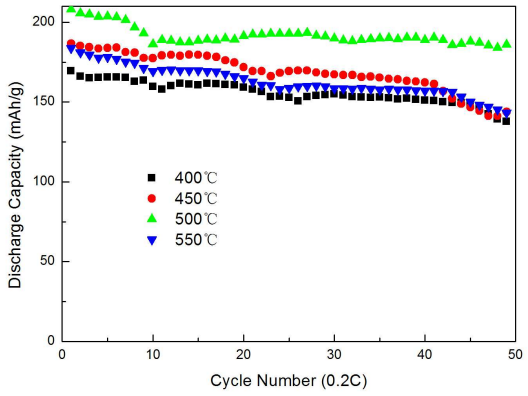

Fig. 11 The cycle performances curves of the $LiNi_{0.8}Co_{0.15}Al_{0.05}O_2$ prepared by precursor powders at different dried temperature (A) 400 °C, (B) 450 °C, (C) 500 °C, (D) 550 °C tested at the room temperature.

Table 4 The cycle performances curves of the $LiNi_{0.8}Co_{0.15}Al_{0.05}O_2$ prepared by precursor powders at different dried temperature (A) 400 °C, (B) 450 °C, (C) 500 °C, (D) 550 °C tested at the room temperature (0.2C).

Sample	Initial discharge capacity (mAh g^{-1})	Discharge capacity (mAh g^{-1}) after 49 cycles	Capacity retention rate (%)
(A)	169.5	137.8	81.29
(B)	186.7	143.9	77.08
(C)	208.0	185.9	89.38
(D)	183.7	143.2	77.95

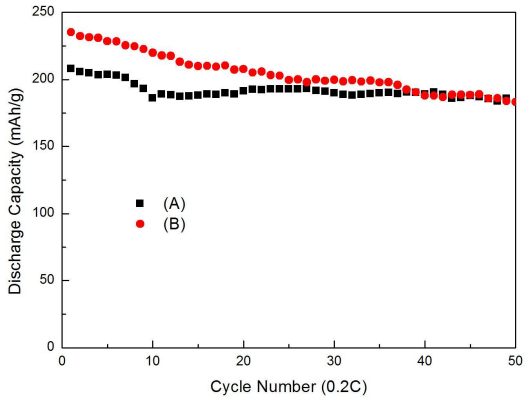

Fig. 12 The cycle performance curves of the mixture of the $LiNi_{0.8}Co_{0.15}Al_{0.05}O_2$ prepared by precursor powders dried at 500 °C and tested at (A) the room temperature, (B) 60 °C (0.2C).

To further prove the stability of the yolk-shell structure of the $LiNi_{0.8}Co_{0.15}Al_{0.05}O_2$, we chose the sample prepared by precursor powders dried at 500 °C, which had the highest BET surface area and discharge capacity and did the cycle retention tested at high temperature above 60 °C at a rate of 0.2 C as shown in Fig. 12. The sample tested at 60 °C showed a higher irreversible capacity about 235.1 mAh g^{-1} s during the first cycle and a worse cycle performance of 78.24 % capacity retention rate after 49 cycle compared to 208.0 mAh g^{-1} and 89.38 % tested at the room temperature.

Conclusions

In summary, the monodisperse crumpled yolk-shell spherical precursors of $LiNi_{0.8}Co_{0.15}Al_{0.05}O_2$ were obtained via a general and simple supersonic atomization method for 10 h at 400 °C to 500 °C, the average diameter from ~1.1 μm to ~1.6 μm, and the initial discharge capacity of the samples which precursor powders dried at 500 °C can reach 225.9 mAh g^{-1} (0.1C) and showed a good cycle performance, which is higher than previously reported. This work provides a facile method for synthesis monodisperse yolk-shell spherical composites applied in Li-ion battery and many other fields.

Acknowledgements

This research was supported by Jiangsu Province prospective joint research on pilot project (No.:BY2013072-03), a Grant for State Key Program for Basic Research of China (Nos.: 2013CB632702, 2012CB921503), the National Natural Science Foundation of China (Nos.: 11134006, 11374149), A Project funded by the Priority Academic Program Development of Jiangsu Higher Education Institutions (PAPD), a Project of Free Exploration funded by National Laboratory of Solid State Microstructures, Test Foundation of Nanjing University.

Notes and references

[a] Nanjing University, National Laboratory of Solid State Microstructures and Department of Materials Science and Engineering, College of Engineering and Applied Sciences, Nanjing 210093, China
[b] Nanjing University, National Laboratory of Solid State Microstructures, School of Physics, Nanjing University, Nanjing 210093, China

*: corresponding author, yftang@nju.edu.cn
Fax: (+)86-25-83594668
E-mail: yftang@nju.edu.cn

† Footnotes should appear here. These might include comments relevant to but not central to the matter under discussion, limited experimental and spectral data, and crystallographic data.
Electronic Supplementary Information (ESI) available: [details of any supplementary information available should be included here]. See DOI: 10.1039/c000000x/

1. J. R. Dahn, U. Vonsacken, M. W. Juzkow and H. Aljanaby, *J Electrochem Soc*, 1991, **138**, 2207-2211.
2. T. Ohzuku, A. Ueda and M. Nagayama, *J Electrochem Soc*, 1993, **140**, 1862-1870.
3. T. Ohzuku, A. Ueda and M. Kouguchi, *J Electrochem Soc*, 1995, **142**, 4033-4039.
4. H. Arai, S. Okada, Y. Sakurai and J. Yamaki, *Solid State Ionics*, 1998, **109**, 295-302.
5. S. Madhavi, G. V. S. Rao, B. V. R. Chowdari and S. F. Y. Li, *J Power Sources*, 2001, **93**, 156-162.
6. S. H. Park, K. S. Park, Y. K. Sun, K. S. Nahm, Y. S. Lee and M. Yoshio, *Electrochim Acta*, 2001, **46**, 1215-1222.
7. J. M. Tarascon and M. Armand, *Nature*, 2001, **414**, 359-367.
8. M. Guilmard, C. Pouillerie, L. Croguennec and C. Delmas, *Solid State Ionics*, 2003, **160**, 39-50.
9. C. H. Chen, J. Liu, M. E. Stoll, G. Henriksen, D. R. Vissers and K. Amine, *J Power Sources*, 2004, **128**, 278-285.
10. P. H. Duvigneaud and T. Segato, *J Eur Ceram Soc*, 2004, **24**, 1375-1380.
11. M. J. Wang and A. Navrotsky, *Solid State Ionics*, 2004, **166**, 167-173.
12. G. V. Zhuang, G. Y. Chen, J. Shim, X. Y. Song, P. N. Ross and T. J. Richardson, *J Power Sources*, 2004, **134**, 293-297.
13. C. V. Ramana, K. Zaghib and C. M. Julien, *J Power Sources*, 2006, **159**, 1310-1315.
14. S. H. Ju, H. C. Jang and Y. C. Kang, *Electrochim Acta*, 2007, **52**, 7286-7292.
15. B. C. Park, H. B. Kim, H. J. Bang, J. Prakash and Y. K. Sun, *Ind Eng Chem Res*, 2008, **47**, 3876-3882.
16. S. Yoon, C. W. Lee, Y. S. Bae, I. Hwang, Y. K. Park and J. H. Song, *Electrochem Solid St*, 2009, **12**, A211-A214.
17. K. K. Chang, B. Hallstedt and D. Music, *Chem Mater*, 2012, **24**, 97-105.
18. I. Hwang, C. W. Lee, J. C. Kim and S. Yoon, *Mater Res Bull*, 2012, **47**, 73-78.
19. G. R. Hu, W. M. Liu, Z. D. Peng, K. Du and Y. B. Cao, *J Power Sources*, 2012, **198**, 258-263.
20. Y. S. Jang, J. H. Kim, J. K. Lee, B. K. Park and Y. C. Kang, *Int J Electrochem Sc*, 2012, **7**, 12370-12382.
21. Z. W. Seh, W. Y. Li, J. J. Cha, G. Y. Zheng, Y. Yang, M. T. McDowell, P. C. Hsu and Y. Cui, *Nat Commun*, 2013, **4**.
22. S. H. Choi and Y. C. Kang, *Chem-Eur J*, 2013, **19**, 17305-17309.
23. C. M. Sim, S. H. Choi and Y. C. Kang, *Chem Commun*, 2013, **49**, 5978-5980.

